ELSEVIER

A numerical study of three-dimensional wall-bounded flows

Gary N. Coleman, John Kim, and Anh-Tuan Le
Mechanical and Aerospace Engineering Department, University of California, Los Angeles, Los Angeles, CA, USA

Nonequilibrium three-dimensional (3-D) turbulent boundary layers are studied using direct numerical simulation (DNS). Time-developing flows are used to investigate the physics of spatial-developing ones. We find that application of a spanwise shear leads to the reduction of both the turbulent kinetic energy and drag, with the most dramatic reduction of the latter occurring when the shear is applied between $y^+ \approx 5$ and 15. When the three-dimensionality is produced by transverse skewing, the resulting alteration of the relationship between the Reynolds stresses is associated in large part with the effect of the pressure gradient upon the amplification or attenuation of the turbulent kinetic energy.

Keywords: turbulence; direct numerical simulation; channel flow; three-dimensional boundary layers

Introduction

Flows over swept-wing aircraft, within turbomachines, and over hulls of marine vehicles all share a common feature: their velocities change not only magnitude but also direction with distance from the surface. Thus, they can all be classified as three-dimensional (3-D) boundary layers (3DBL), the subject of the present study. Here our attention is limited to the nonequilibrium case, in which the 3DBL is created by an abrupt change of the mean flow to which the turbulence has not yet adjusted. This choice is motivated by its relevance to many technically important flows (such as the three cited above), and by the fact that the physics of nonequilibrium 3DBLs is not well understood. For example, when an initially two-dimensional (2-D) equilibrium boundary layer is suddenly subjected to a spanwise shearing force by the impulsive motion of the surface, the resulting nonequilibrium flow can experience a *decrease* of turbulent kinetic energy (see below); because the addition of a mean strain typically causes the turbulence to become *more* energetic, this behavior is somewhat paradoxical. On the other hand, when the mean streamwise vorticity appears, not because of a moving wall, but by skewing of spanwise vorticity with a transverse strain (such as that produced by a curved duct) that deflects the entire layer, the turbulent kinetic energy has been observed to both increase (Schwarz and Bradshaw 1994) and decrease (Bradshaw and Pontikos 1985), presumably depending upon the nature of the streamwise pressure gradient. Moreover, regardless of whether the three-dimensionality is due to surface shear or transverse straining (i.e., for both the "shear-driven" and "pressure-driven" versions), the "structure" of the Reynolds stresses is usually altered, because the ratio of the turbulent shear stress magnitude to the turbulent kinetic energy decreases. This implies that turbulence in nonequilibrium 3DBLs is "less efficient" at extracting energy from the mean.

These observations illustrate the difficulty associated with correctly modeling 3DBLs. Another problem, related to the "structural" one mentioned above, is that as the turbulence reacts to the imposed crossflow, the Reynolds stresses do not instantaneously adjust to changes in the mean shear. Therefore, models based on an isotropic eddy-viscosity, or, indeed, any concept developed for 2-D equilibrium boundary layers, cannot, in general, be assumed to be valid for this flow. It is hoped that this study, in which we perform numerical experiments on "canonical" 3DBLs in an attempt to isolate various effects of three-dimensionality, will remove some of these modeling uncertainties by improving our understanding of the physics of nonequilibrium 3DBLs.

Approach

Three flow configurations are considered, with the mean three-dimensionality created by shear for the first two, and by transverse strain for the third. All three assume a plane channel geometry and are studied using direct numerical simulation (DNS); because all relevant scales of motion are resolved, no turbulence or subgrid-scale model is needed. The shear-driven cases (denoted here by an SD prefix) are the result of impulsive motion of the lower channel wall, either by suddenly imposing a constant spanwise velocity w_s upon fully developed 2-D Poiseuille flow or by suddenly stopping the wall after the turbulence has adjusted to the wall motion. The runs subjected to transverse strain (indicated by prefix *TS*) utilize a constant uniform irrotational mean deformation $dU/dx = -dW/dz$ in the streamwise–spanwise (x–z) plane. This deformation represents either a streamwise expansion or contraction, and thus corresponds to either a favorable or adverse streamwise pressure gradient in a boundary layer. (The actual streamwise pressure gradient is

Address reprint requests to Dr. G. N. Coleman, Mechanical and Aerospace Engineering Department, University of California, Los Angeles, 48-121 Engr. IV, Box 951597, Los Angeles, CA 90095-1597, USA.

Received 6 November 1995; accepted 30 January 1996

Int. J. Heat and Fluid Flow 17: 333–342, 1996

655 Avenue of the Americas, New York, NY 10010

0142-727X/96/$15.00
PII S0142-727X(96)00042-2

turned off during the straining.) Therefore, it produces, for a flow with nonzero mean spanwise velocity $\overline{w}$, a skewed 3-D boundary layer that allows, for example, investigation of the "inviscid skewing" mechanism (Bradshaw 1987). (Throughout this paper, the terms streamwise and spanwise are used respectively to indicate the x- and z-directions, and and u- and w-components of velocity, even when the x-axis does not correspond to the actual downstream direction of the mean flow; the y-coordinate denotes the wall-normal direction, and v, the wall-normal velocity.) Whereas previous DNS studies have assumed both the strain and turbulence were homogeneous (Rogallo 1981), here we apply the uniform strain to turbulence between two no-slip surfaces. For this we deform both the flow and the (elastic) channel walls. Consequently, the near-wall turbulence for the present and actual skew-induced 3-D boundary layers will not always correspond. Nevertheless, because the outer flow behavior is of primary interest for this type of 3DBL, the transversely strained results are expected to be useful, especially for differentiating between physics of the shear-driven and pressure-driven cases.

The results to follow have been obtained using the spectral channel-flow code of Kim et al. (1987), after it was modified to compute the cases described above. All variables are nondimensionalized by the channel half-width δ^*, and (in order to highlight changes in time) the constant wall-shear velocity from the 2-D Poiseuille flow initial condition. Because of the time-dependence of the results, mean quantities (denoted by an overbar) are obtained by averaging over planes parallel to the walls, and for Case SD1 also over three independent simulations. A summary of case parameters is given in Table 1. In addition to those listed, a series of runs using a time-independent spanwise shear are also discussed (see Table 2 below). Three sets of numerical parameters are used: for Cases SD1, SD2, TS1, and TS2, the streamwise and spanwise domain size L_x^* and L_z^* are $4\pi\delta^*$ and $8\pi\delta^*/3$,

Table 1 Case parameters

Case	w_s	u_s	dU/dx	IC
SD1	−8.5	0	0	2D*
SD2	0	0	0	collateral†
SD3	0	+8.5	0	2D*
TS1	−8.5	0	−100	collateral†
TS2	−8.5	0	+100	collateral†

*Kim et al. (1987); †Case SD1 at $t = 1.73$

Notation

a_1	Reynolds stress structure parameter, $(\overline{u'v'}^2 + \overline{v'w'}^2)^{1/2}/q^2$
dU_i/dx_j	constant uniform rate of irrotational strain
h	height below which constant spanwise shear is applied
L_x^*, L_z^*	streamwise and spanwise dimensions of computation domain, respectively
n_x, n_y, n_z	number of equivalent grid points in the streamwise, wall-normal, and spanwise directions, respectively
q^2	twice the turbulent kinetic energy, $\overline{u_i'u_i'}$
Re_τ	Reynolds number, $(u_\tau^*)_{ic}\delta^*/\nu^*$
S	magnitude of strain rate, $\lvert dU_i/dx_j\rvert$
t	nondimensional time, $t^*(u_\tau^*)_{ic}/\delta^*$
T	oscillation period of spanwise pressure gradient or spanwise wall motion
u, v, w	nondimensional streamwise, wall-normal, and spanwise velocity components, respectively, $(u^*, v^*, w^*)/(u_\tau^*)_{ic}$
$\overline{u}, \overline{w}$	mean streamwise and spanwise velocities, respectively
$\overline{u'v'}, \overline{v'w'}$	streamwise and spanwise Reynolds shear stresses, respectively
u_s, w_s	constant streamwise and spanwise velocities of lower channel wall, respectively
$(u_\tau^*)_{ic}$	mean surface friction velocity of initial fully developed 2-D Poiseuille flow field
x, y, z	nondimensional streamwise, wall-normal, and spanwise coordinates, respectively, $(x^*, y^*, z^*)/\delta^*$
y_w	distance from lower wall, $(\delta^* + y^*)/\delta^*$
y^+	nondimensional distance from the wall, $y_w^* u_\tau^*/\nu^*$

Greek

α	local skewing angle, $\arctan(St)$
β	angle between the collateral flow and local skewing directions
δ^*	half-width of channel
ε	rate of dissipation of turbulent kinetic energy
ζ	Stokes's second problem similarity variable, $y^+(\pi)^{1/2}/(T^+)^{1/2}$
η	Stokes's first problem similarity variable, $y_w^*/2(\nu^* t^*)^{1/2}$
θ	angular difference in orientation of skewed mean vorticity between cases with and without initial component of mean vorticity in pure skewing direction, as predicted by generalized Squire-Winter-Hawthorne relationship
λ	angle between mean shear and Reynolds stress, $\arctan[(\partial\overline{w}/\partial y)/(\partial\overline{u}/\partial y)] - \arctan(\overline{v'w'}/\overline{u'v'})$
ν^*	kinematic viscosity
ξ	eddy-viscosity ratio, $[\overline{v'w'}/(\partial\overline{w}/\partial y)]/[\overline{u'v'}/(\partial\overline{u}/\partial y)]$
$(\overline{\tau}_x, \overline{\tau}_z)_w$	mean streamwise and spanwise shear, respectively, at $y^* = \pm\delta$ (averaged over both walls)
ω_i	vorticity, $\omega_i^*/[(u_\tau^*)_{ic}/\delta^*]$

Indices

Q^*	dimensional quantity
Q^+	quantity nondimensionalized by u_τ^* and ν^*
$\overline{Q}$	average over (x, z)-planes (and where noted, over independent simulations)
Q'	fluctuation component, $Q - \overline{Q}$
Q_c	variable measure at channel centerline
Q_w or Q_s	value of Q at lower wall, $y^* = -\delta^*$
Q_{ic}	value from initial fully developed 2-D Poiseuille flow field

respectively, while the number of streamwise (n_x) wall-normal (n_y), and spanwise (n_z) grid points is $(n_x, n_y, n_z) = (256, 129, 256)$; Case SD3 uses $(L_x^*, L_z^*) = (4\pi\delta^*, 4\pi\delta^*/3)$ and $(n_x, n_y, n_z) = (128, 129, 128)$, while $(L_x^*, L_z^*) = (4\pi\delta^*, 4\pi\delta^*/3$ and $(n_x, n_y, n_z) = (32, 65, 32)$ for the constant spanwise-shear simulations. The results presented below verify that with these parameters all essential scales of motion are fully resolved (see, for example, Figures 5, 6, 7, and 12, and compare diagnostics discussed in Kim et al.).

Results: shear-driven cases

Spanwise moving wall ($w_s \neq 0$)

Three-dimensional boundary layers free of adverse pressure gradient effects can be created by introducing mean streamwise vorticity at the surface. We begin our examination of this so-called shear-driven case with Run SD1, for which an impulsive spanwise motion is applied to the lower wall of a stationary 2-D plane channel flow—hence, the '2-D' in the "IC" column in Table 1. The fully developed initial field is as described in Kim et al. (1987), with Reynolds number based on surface friction velocity and channel half-width $\mathrm{Re}_\tau \approx 180$. The boundary layer that develops above the moving wall is analogous to that found in rotating cylinder experiments (Furuya et al. 1966; Lohmann 1976; Driver and Hebbar 1991) in the region where the longitudinal flow along the cylinder first encounters the rotating section. It is also similar to that found by Moin et al. (1990) and Sendstad and Moin (1992), who used DNS to study the transient response of a 2-D channel flow to a suddenly imposed spanwise pressure gradient. This similarity is no surprise, given that the effect of the spanwise pressure gradient is equivalent (because of the streamwise homogeneity of the plane channel) to subjecting the walls to a uniform spanwise acceleration. Many of the results found here are qualitatively similar to those found earlier by Sendstad and Moin. There are fundamental differences, however, between the accelerating and constant-velocity wall flows: the equilibrium state of the former is a reoriented Poiseuille flow, while here the moving wall leads first to an equilibrium "collateral" boundary layer (a flow for which the (new) direction of the mean velocity remains constant in y), and eventually—once the spanwise shear diffuses across the channel centerline to the stationary wall—to an equilibrium skewed 3DBL Poiseuille/Couette configuration (because the direction of the mean velocity varies approximately linearly in y). (Had we set both walls in motion in the same direction, the final state would have been two equilibrium collateral boundary layers.) In this paper, we consider times shorter than those required for the spanwise mean shear to diffuse across the centerline; therefore, only the nonequilibrium-to-collateral transition. Another difference between the present and Sendstad and Moin's study is that, because they were interested only in the nonequilibrium state, their domain size and numerical resolution were insufficient to capture their reoriented 2-D flow accurately, with its associated smaller streamwise scales. Here, however, because of the central role played by the collateral boundary layer, it is necessary to use numerical parameters sufficient to correctly represent both the transient and long-time behaviors.

The imposed spanwise wall velocity for Case SD1, $w_s = -8.5$, is about half the initial mean streamwise velocity at the centerline $\bar{u}_c$ [and, therefore the collateral flow angle will be about $26^\circ \approx \arctan(0.5)$]. To avoid a discontinuity in y, an early-time Stokes solution for the impulsively started flat plate is used to specify the initial distribution of $\bar{w}(y)$. At this Reynolds number, the $\bar{w}$-profile imposed at $t = 0$ corresponds to the Stokes solution at $t = 0.0045$. The resulting variation in time of the mean spanwise velocity profile is shown in Figure 1a. The solid curves represent an average over planes parallel to the walls and over three independent realizations beginning from three different initial fields. The dotted curve illustrates the Stokes solution at the time corresponding to the last ensemble-averaged result ($t = 0.750$). Even at this last time, the laminar and turbulent profiles are not drastically different; at $t = 0.375$ the agreement between the Stokes solution (not shown), and the Case SD1 profile is significantly better—a consequence of the slow development of the spanwise Reynolds stress $\overline{v'w'}$. The dashed curve in Figure 1a shows the spanwise velocity at $t = 1.73$. As the polar

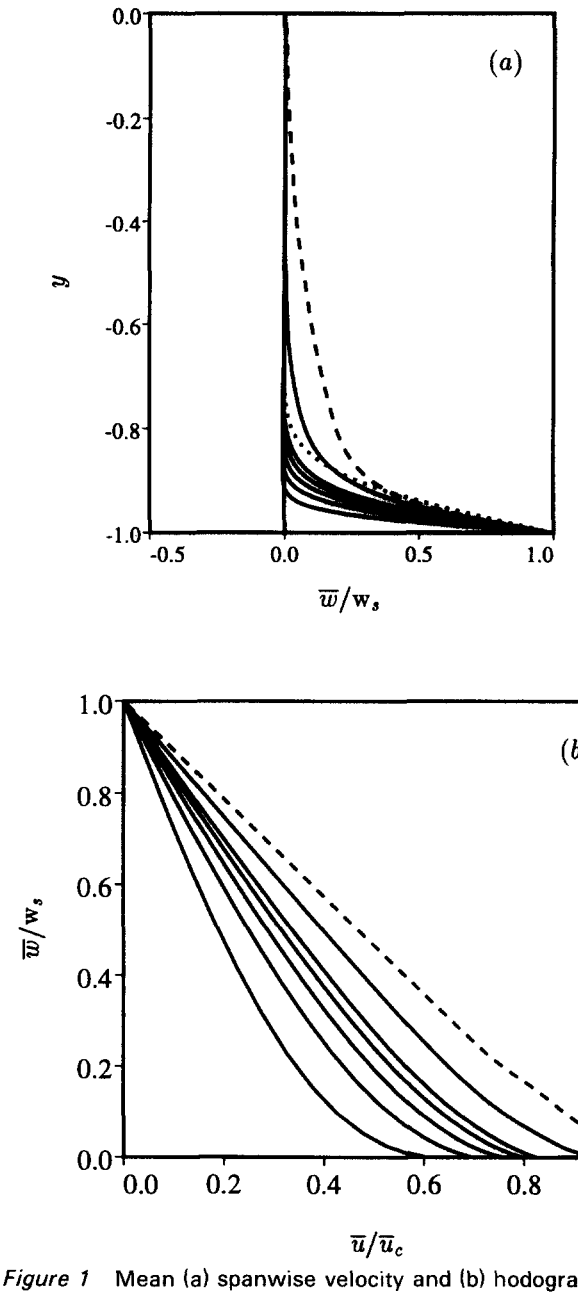

Figure 1 Mean (a) spanwise velocity and (b) hodograph for Case SD1: ——, ensemble average over three independent realizations for time sequence $t = 0.075, 0.150, 0.225, 0.300, 0.375$, and 0.750; - - - - -, laminar Stokes solution at $t = 0.75$; – – – –, plane average over single realization at $t = 1.73$; time normalized by channel half-width and surface friction velocity from initial field

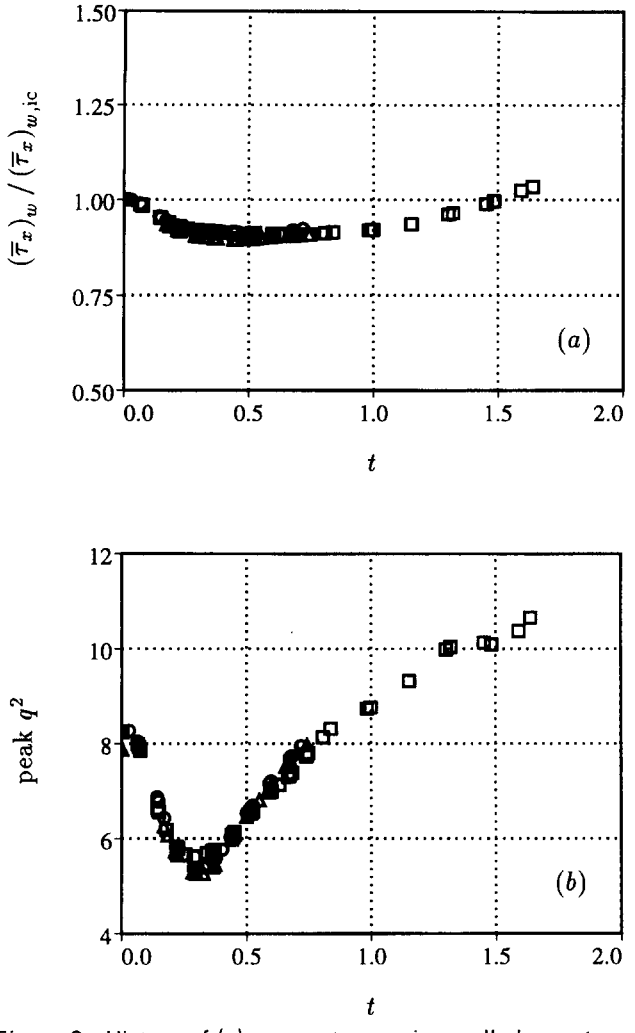

Figure 2 History of (a) mean streamwise wall shear stress (normalized by initial value) and (b) maximum q^2 for Case SD1: symbols denote planar averages from three independent realizations

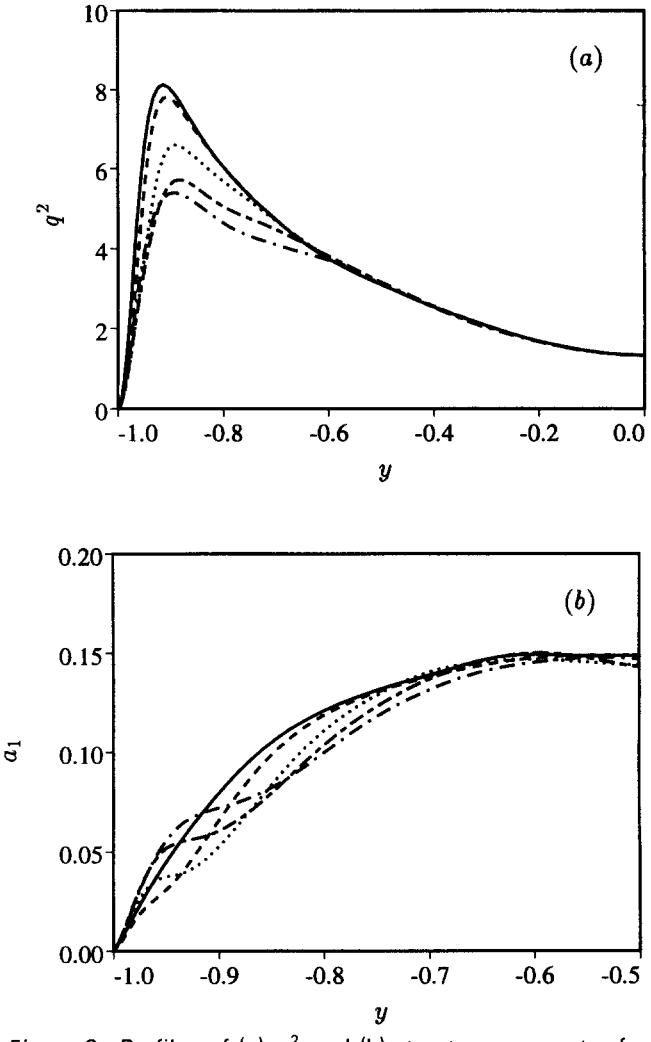

Figure 3 Profiles of (a) q^2 and (b) structure parameter for Case SD1: ——, $t=0$; - - - - -, $t=0.075$; · · · · ·, $t=0.150$; — — —, $t=0.225$; — - —, $t=0.300$; structure parameter $a_1 = [(\overline{u'v'})^2 + (\overline{v'w'})^2]^{1/2}/q^2$; ensemble average over three realizations

velocity plot in Figure 1b indicates (because the direction of the mean velocity is very nearly constant with distance from the surface) the flow at this time is to a good approximation collateral. The $t = 1.73$ field is used as initial conditions for some of the cases described below (see Table 1).

Adding a spanwise component to the shear at the wall causes a reduction in the streamwise component, as Figure 2a shows. The streamwise wall shear drops to a minimum of about 90% of its initial value before the added shear leads to its eventual growth. (Simulations other than those presented here indicate that imposing a larger shear produces a larger wall-shear reduction than found for Case SD1.) The drop in turbulent kinetic energy $(1/2)q^2 = (1/2)\overline{u_i'u_i'}$, associated with the wall-shear decrease can be seen in Figure 3a. The effect spreads away from the wall in time, as more and more of the layer experiences a drop in q^2 as time passes. A trace of the history of the near-wall peak of q^2 is presented in Figure 2b. Its behavior is similar to that of the wall shear, in that an initial reduction precedes growth to greater than initial values. The maximum q^2 begins to grow sooner than the wall shear does, however.

Figure 3b shows how the relationship between the components of the Reynolds stress tensor is altered by the spanwise shear: the structure parameter a_1 is significantly reduced. This reduction, which is a central feature of nonequilibrium 3DBLs, implies that for the shear-driven case the decrease in magnitude of the lateral shear stress is even more rapid than that of the turbulent kinetic energy. Note that the shear-induced reduction of both a_1 and q^2 propagates away from the wall in time. The finite lag between the angles of the mean shear and shear stress (Figure 4a) is such that, while they eventually coincide as the collateral state is approached, initially the two angles differ by almost 40°. The shear always "leads" the stress so that $\arctan[(\partial\overline{w}/\partial y)/(\partial\overline{u}/\partial y)] - \arctan(\overline{v'w'}/\overline{u'v'})$ remains positive. A more straightforward demonstration of the difficulty associated with using a scaler eddy-viscosity to model this flow is presented in Figure 4b, which illustrates the evolution of the ratio of the spanwise to streamwise eddy-viscosity; only after q^2 begins to grow (cf. Figures 2b and 4b) does this ratio begin to approach one.

The spatial structure of the turbulence is also modified by the moving wall. We find that the smallest scales of motion adjust most rapidly to changes in mean flow conditions. This observation, which was previously made by Sendstad and Moin (1992) in

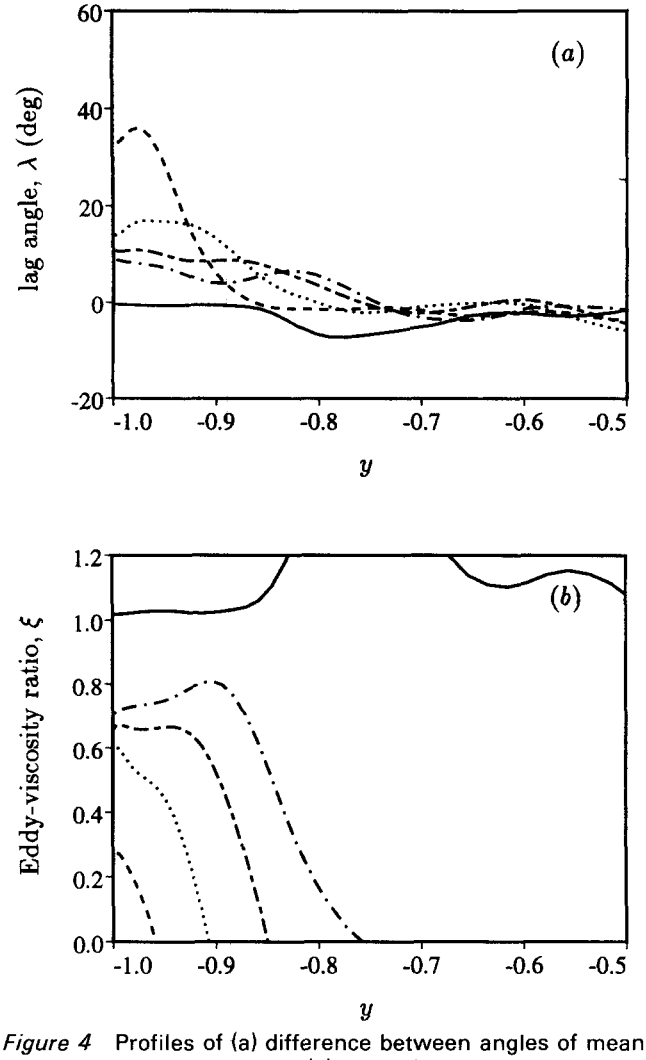

Figure 4 Profiles of (a) difference between angles of mean shear and shear stress and (b) ratio of spanwise to streamwise eddy-viscosity for Case SD1: ——, $t=1.73$; other symbols as in Figure 3. Lag angle, $\lambda=\arctan[(\partial\overline{w}/\partial y)/(\partial\overline{u}/\partial y)]-\arctan(\overline{v'w'}/\overline{u'v'})$; eddy-viscosity ratio, $\xi=[\overline{v'w'}/(\partial\overline{w}/\partial y)]/[\overline{u'v'}/(\partial\overline{u}/\partial y)]$

their 3DBL DNS study, is supported by the two-dimensional energy spectra shown in Figure 5. These spectra also indicate the numerical fidelity of the DNS results, over the entire 2-D-to-collateral flow range. (The same conclusion is also reached when the one-dimensional (1-D) spectra (not shown here) are examined.) At this y-location (which in wall units initially corresponds to $y^+\approx 15$), the high-level contours at low wavenumbers are "turned" more slowly than are their low-level high-wave number counterparts. The enstrophy profiles in Figure 6a also imply that at this location ($y=-0.92$) the smaller scales initially become more energetic. Part of the previously noted drop in the peak q^2 —in addition to being the result of reduced production caused by lower mean shear and turbulent shear stress (Figures 2a and 3b) —is, therefore, due to an increase in the rate of turbulent kinetic energy dissipation ε. Near the wall, however, the vorticity fluctuations weaken in time, indicating that here the energy at smaller scales (and, hence, the dissipation rate) is diminished. The time-dependent influence of the spanwise shear on the location of the maximum enstrophy can be accounted for to some degree by using the similarity variable of the laminar Stokes solution, $\eta=y_w^*/2(\nu^* t^*)^{1/2}$ (using the $*$ superscript to denote dimensional variables, with ν^* the kinematic viscosity, and $y_w^*=\delta^*+y^*$), to rescale the wall-normal coordinate. When this is done (Figure 6b) the enstrophy maximum is found for the times considered to remain near $\eta\approx 1$.

More instantaneous structural information is available in Figure 7, which shows contours of wall-normal vorticity in x–z planes just above the moving wall from one of the Case SD1 realizations, revealing the effect of the imposed spanwise shear upon the streaks. They are first weakened and "torn" into smaller structures; later they become stronger and more elongated as they realign in the collateral flow direction.

A complication in the analysis of Case SD1 is the time-dependent nature of the imposed mean spanwise shear. Although some of the time-dependence can be removed by using laminar theory, as in Figure 6b, the fact that $\partial\overline{w}/\partial y$ varies in both y and t makes it difficult to determine the mechanisms responsible for, for example, the turbulent drag reduction, because different near-wall structures exist at different y^+ locations. We have, therefore, performed a series of runs using "synthetic" time-independent mean spanwise velocities: a uniform spanwise shear $\mathrm{d}\overline{w}/\mathrm{d}y$ of equal magnitude is applied over various regions, and held constant in time. Because we are primarily interested in the initial response of the turbulence to the applied shear, we do not allow the imposed initial $\overline{w}$ profile to change in time under the influence of viscosity, and the turbulence; $\mathrm{d}\overline{w}/\mathrm{d}y$ is held fixed to make comparisons more straightforward than they would be if $\overline{w}$ evolved naturally. Because our attention is upon near-wall behavior, it is possible to specify a lower-Reynolds number for these runs than was used to obtain the Case SD1 results described above. Instead of 180, here the initial Re_τ is 112. This greatly reduces the computational expense, because at $\mathrm{Re}_\tau=112$ only $(n_x,n_y,n_z)=(32,65,32)$ collocation points are required, which allows us to explore a wider parameter range for a given amount of CPU time than would be possible at higher-Reynolds numbers. (We have also used the "minimal channel" geometry (Jiménez and Moin 1991) to investigate the effect of constant spanwise shear upon 2-D channel flow. However, because in the present study we choose to impose $\mathrm{d}\overline{w}/\mathrm{d}y$ at locations fairly far away from the walls, those results are not presented here, in order to avoid uncertainties that might be present in minimal-channel statistics from far-wall regions.)

Three series of constant-shear simulations were made; these are denoted by a CSD prefix and summarized in Table 2. Each series uses a distinct value of constant $\mathrm{d}\overline{w}/\mathrm{d}y$ (either 50, 200, or 800% of the initial mean streamwise wall shear), and contains eight individual runs, which are defined by the height h above the wall over which $\mathrm{d}\overline{w}/\mathrm{d}y$ is imposed. The region of uniform shear extends from the surface to h^+, measured in wall-units of the initial 2-D field, which varies from 5 to 40 in increments of 5. To prevent a discontinuity in the $\overline{w}$ profile, above $1-|y|=h$ the spanwise shear drops to zero as a Gaussian that falls to 1% of its nominal value over five initial wall units. The shear is applied over both sides of the channel, so that both walls are set in motion in the same direction at a constant spanwise velocity proportional to $h\,\mathrm{d}\overline{w}/\mathrm{d}y$.

A comparison of mean streamwise surface drag histories is shown in Figure 8; a reduction with time is found in all instances, with the drop proportional to the magnitude of the applied shear (cf. Figure 8a, b, and c). The weakest effect occurs when the shear is imposed between $y_{ic}^+=0$ and 5 (y_{ic}^+ is the wall-normal coordinate in wall-units of the initial field), with a cumulative drag reduction as the depth of the sheared region increases. Note, however, that once the shear extends beyond $y_{ic}^+\approx 25$ for the weakest shear (Series CSD1; Figure 8a), and $y^+\approx 15$ for the largest $\mathrm{d}\overline{w}/\mathrm{d}y$ (Series CSD3; Figure 8c), further increases in h^+

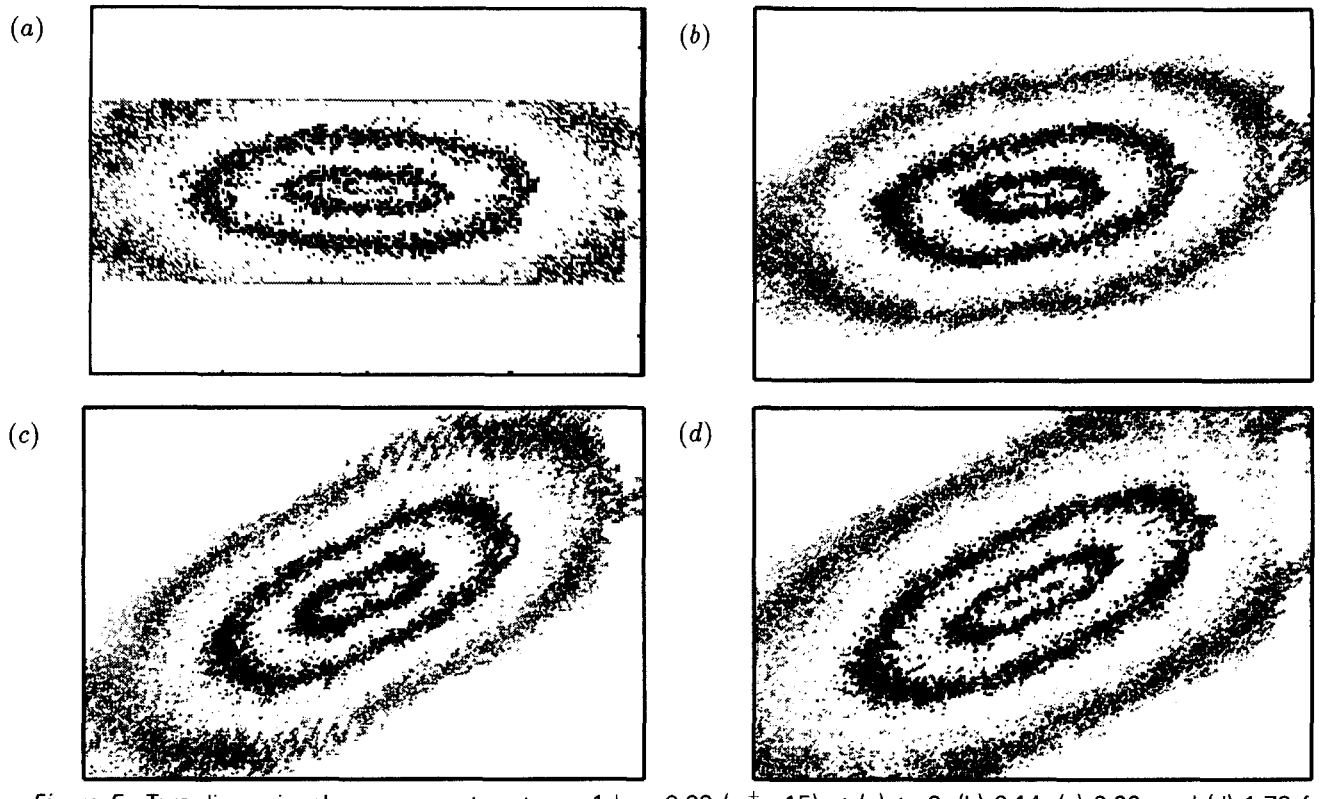

Figure 5 Two-dimensional energy spectra at $y_w = 1 + y = 0.08$ ($y_{ic}^+ \approx 15$) at (a) $t = 0$, (b) 0.14, (c) 0.29, and (d) 1.73 for one realization of Case SD1: contours indicate constant values, in intervals of -1.8, of logarithm of spectra, normalized by maximum value at each time; horizontal and vertical axes are spanwise and streamwise wave numbers, respectively, with mean mode at center

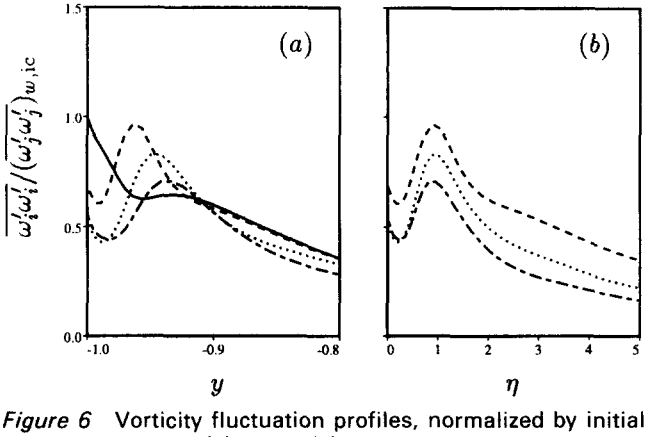

Figure 6 Vorticity fluctuation profiles, normalized by initial wall value, *versus* (a) y and (b) η for Case SD1: symbols as in Figure 3

do not lead to a significant change in the rate of drag decrease. Moreover, the greatest "jump" in the drag reduction occurs when h^+ moves from $y_{ic}^+ = 10$ to 15 for the weak shear runs (CSD1), and from $h^+ = 5$ to 10 for Series CSD3, for which $d\overline{w}/dy$ is largest. This indicates that the "optimal shearing"—that which most deeply disrupts the 2-D equilibrium state—is application of $d\overline{w}/dy$ to the region between $y^+ \approx 5$ and 15, with a tendency for the "critical region" to shift towards the lower limit as the spanwise shear increases.

In the version of this paper presented at TSF-10, the upper limit of the range of maximum influence was found to be $y^+ \approx 10$, not $y^+ \approx 15$, as it is here. This is because there instead of considering histories of mean surface shear stress, turbulent kinetic energy histories were analyzed. It was subsequently discovered that the development of the streamwise surface drag is a better measure of 3DBL behavior, because it is less sensitive than q^2 to the magnitude of the applied spanwise shear; at very large shear rates, the surface drag and kinetic energy histories show opposite trends, with the former decreasing in time, while the latter experiences rapid growth. (Another, less significant, reason for the difference is that the q^2-histories previously presented were not taken from the minimal-channel runs described earlier, as claimed, but from preliminary course-grid simulations; however, because results from the two runs were quite similar, the influence of this error was slight.)

These constant-shear findings are perhaps related to the effect of an oscillating spanwise mean pressure gradient (or equivalently spanwise oscillating walls) upon turbulent boundary layers. Numerical (Jung et al. 1992) and experimental (Laadhari et al. 1994) studies have shown that maximum suppression of turbulence occurs when the spanwise oscillation period in wall units is about $T^+ = 100$. Because of the applicability of the laminar theory for the mean spanwise velocity for the oscillating wall flow (Jung et al.), a connection can be made between the $T^+ \approx 100$ optimum, and the above observation that shear below $y^+ = 15$ is most effective: at $T^+ = 100$ and $y^+ = 15$, the similarity variable ζ for the laminar solution, which can be written as $\zeta = y^+(\pi)^{1/2}/(T^+)^{1/2}$, gives $\zeta/(\pi)^{1/2} = 1.5$, which is close to the effective depth of the boundary layer created by the oscillating wall, as shown in Figure 9.

Finally, we comment on the significance of the present results for theories regarding the structural mechanisms responsible for

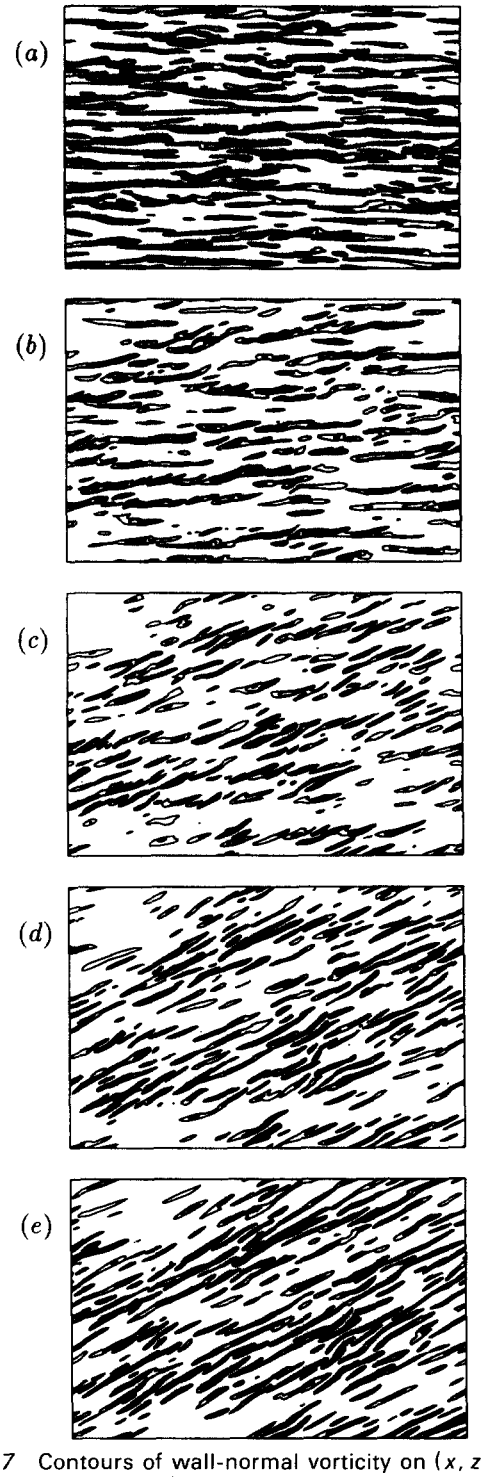

Figure 7 Contours of wall-normal vorticity on (x, z)-planes at $y_w = 1 + y = 0.003$ ($y_{ic}^+ \approx 0.5$) at (a) $t = 0$, (b) 0.075, (c) 0.150, (d) 0.225, and (3) 0.300 for one realization of Case SD1: ——, $\omega_y > 0$; contour interval = 1; flow at centerline from left to right; spanwise wall motion from top to bottom; planes represent full flow domain

the drag reduction in shear-driven 3DBLs. One suggestion is that the reduction is due to the spanwise shear directly modifying the near-wall quasi-streamwise vortices, thereby weakening the energy production cycle (Eaton 1995). Although the present results are not inconsistent with this theory, because on average, the quasi-streamwise vortices are found near $y^+ = 20$ (which is just above the "optimal shearing" region of $5 < y^+ < 15$), the greatest influence of shear-driven three-dimensionality appears to be due to modification of the "bottoms of" the vortices, the "tops of" the streaks, or of the *interaction* between the two. We also note that applying a spanwise shear in the region below $y^+ = 5$ produces a smaller drag reduction than when $d\bar{w}/dy$ is imposed between $y^+ \approx 15$ and 25 (Figure 8), which suggests that the weakening and "shredding" of the streaky structure observed *very* near the wall at $y_{ic}^+ \approx 0.5$ (Figure 7) is more a symptom of the tree-dimensionality than an important part of the dynamics.

Table 2 Constant spanwise-shear runs

Series	$\frac{d\bar{w}}{dy} \Big/ \left(\frac{\partial \bar{u}}{\partial y}\right)_{w,ic}$
CSD1	0.5
CSD2	2.0
CSD3	8.0

Stationary wall ($w_s = 0$)

The other type of shear-driven 3DBL considered here also has an analog in the rotating cylinder experiments: by suddenly stopping the spanwise-moving wall in the channel after a collateral state has developed, an effect comparable to passing from the rotating to stationary section in the experiments is produced. The initial condition for this stopped-wall run, Case SD2, is obtained from Case SD1 at $t = 1.73$. As can be seen from the

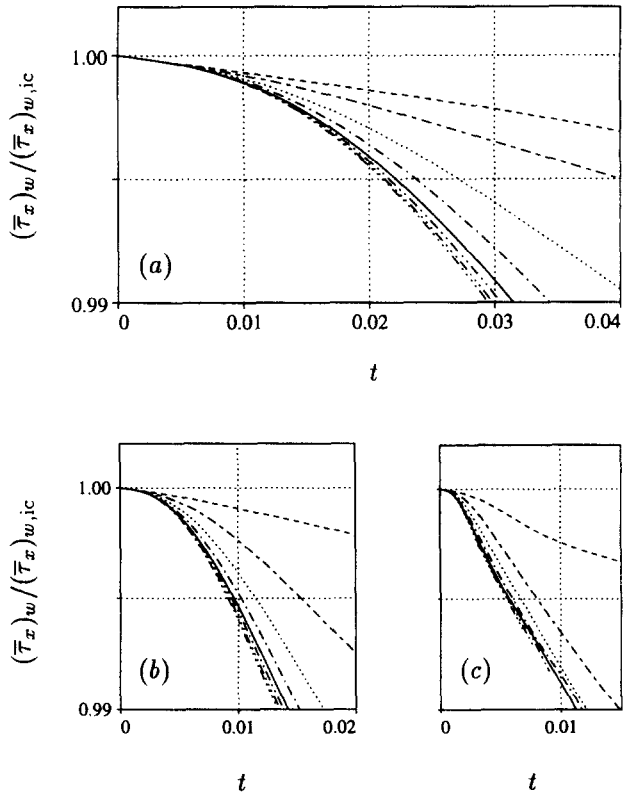

Figure 8 History of mean streamwise wall shear stress, normalized by initial value, for constant spanwise-shear runs, Series (a) CSD1, (b) CSD2 and (c) CSD3: ----, $h^+ = 5$; — — —, $h^+ = 10$; - - - - -, $h^+ = 15$; — - —, $h^+ = 20$; ——, $h^+ = 25$; — - - —, $h^+ = 30$; — - - - —, $h^+ = 35$; — - - - - —, $h^+ = 40$; results at each time averaged over both walls

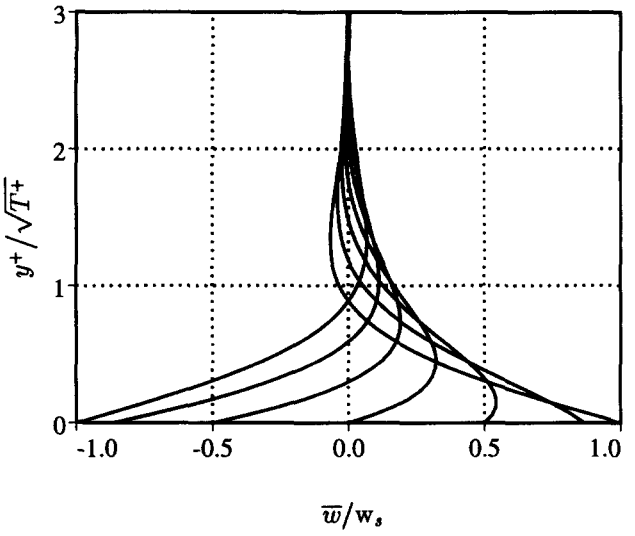

Figure 9 Stokes oscillating flat-plate solution: time sequence over half period in 30° increments

$t = 1.73$ results in the Case SD1 hodograph (Figure 1b) and the kinetic energy spectra (Figure 5d), the layer above the moving wall is effectively 2-D at this time. Thus, when the coordinate system coincides with the angle of the mean shear at the surface (26°), the resulting mean "spanwise" velocity has no y-variation (Figure 10). Consequently, the only difference between subjecting a 2-D boundary layer to an impulsive spanwise wall velocity and suddenly stopping the wall beneath a collateral boundary layer is that in the latter case the imposed wall shear has both a downstream and cross-stream component, the relative strengths of which depend upon the collateral flow angle. Because the applied downstream shear and the existing collateral surface shear are aligned and of opposite sign, the Case SD2 energy-drop (Figure 11) is due to both the cross-flow effect discussed above and also a straightforward reduction in the usual 2-D $-\overline{u'v'}\,\partial\overline{u}/\partial y$ production. However, although both the downstream and cross-stream components act to reduce the turbulent energy, their influence upon the flow structure is fundamentally different. Results from Case SD3, a run for which the lower channel wall is moved solely in the downstream direction, show, for

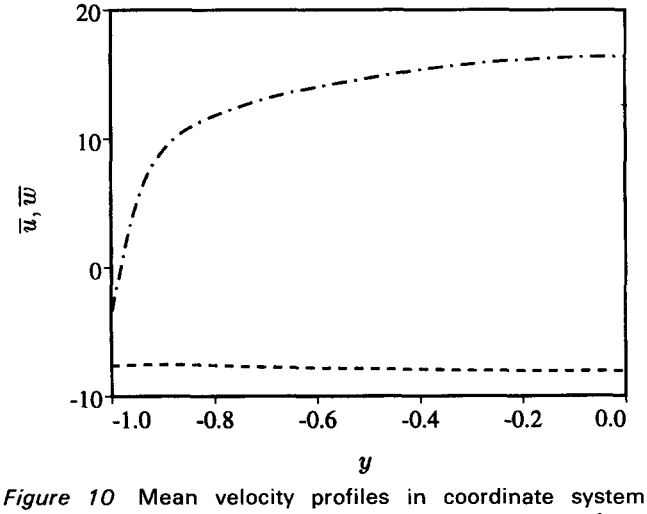

Figure 10 Mean velocity profiles in coordinate system aligned with direction of mean shear angle at the surface, for Case SD2 at $t=0$: —·—, $\overline{u}$; ----, $\overline{w}$

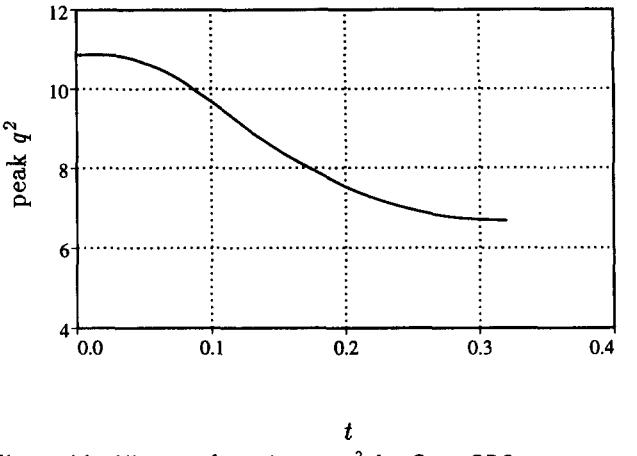

Figure 11 History of maximum q^2 for Case SD2

example, that the vorticity fluctuations are everywhere diminished by the streamwise shear (Figure 12), while the cross-flow (see Figure 6a) leads to an increase at some locations and a decrease at others.

Results: transversely strained cases

We conclude with some preliminary results from the strained channel simulations, Cases TS1 and TS2. The strain rate $S = |dU/dx|$ used for these runs is such that at the channel centerline the nondimensional strain-rate parameter $Sq^2/\varepsilon \approx 160$; this value of S is 48% of the mean shear at the surface, $[(\partial\overline{u}/\partial y)_w^2 + (\partial\overline{w}/\partial y)_w^2)^{1/2}$, of the initial collateral flow (Case TS1 at $t = 1.73$), and therefore represents a very rapid deformation. Note the opposite signs of dU/dx for the two simulations. If the collateral initial state were exactly aligned at 45° to the x-axis, the applied $dU/dx = -dW/dz$ strain would produce a pure irrotational skewing of the flow (i.e., in downstream coordinates the only nonzero terms of the strain rate would be the off-diagonal components $dU/dz = dW/dx$, as if a pressure gradient were acting at a right angle to the mean streamlines), and the only difference between Cases TS1 and TS2 would be that one would turn the flow (in time) to the right, and the other to the left,

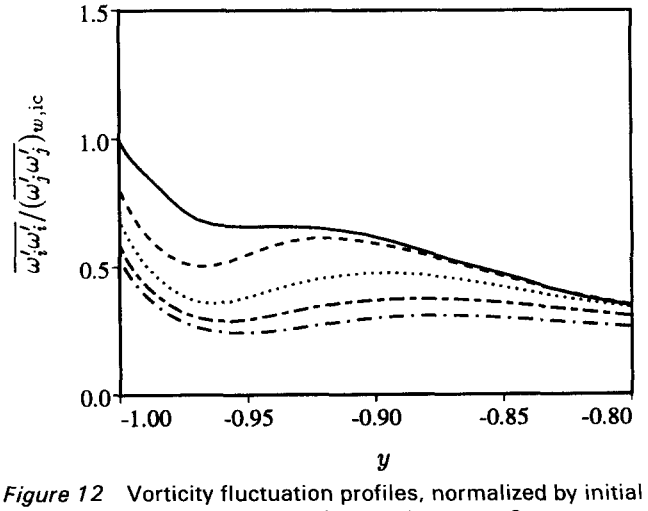

Figure 12 Vorticity fluctuation profiles, normalized by initial wall value, for Case SD3; symbols as in Figure 3

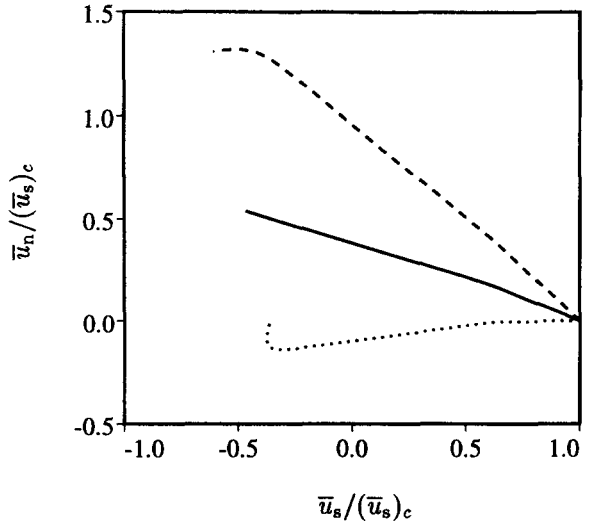

Figure 13 Mean velocity hodograph for Cases TS1 and TS2: ——, $St=0$; – – – –, Case TS1 at $St=0.25$; - - - - -, Case TS2 at $St=0.25$; velocity components parallel $\overline{u}_s$ and normal $\overline{u}_n$ to local coordinates aligned with current direction of mean skewing, normalized by parallel component at centerline $(\overline{u}_s)_c$

respectively. However, because the collateral flow angle is 26°, the opposite signs of dU/dx correspond to a mean deceleration of the boundary layer in the downstream direction for Case TS1 and an acceleration for Case TS2.

Mean velocity hodographs are shown in Figure 13. The velocity components are measured with respect to the coordinate system defined by the turning angle of the irrotational skewing: the downstream direction is at 45° + α clockwise from the x-axis, where the effective turning angle $\alpha = \arctan(-t\,dU/dx)$. This choice allows us to check the validity of a generalized Squire–Winter–Hawthorne relationship for the mean velocity (Bradshaw 1987), derived by assuming that in the outer layer the evolution of the mean vorticity is simply given by skewing of vortex lines in the x–z plane (and taking into account that initially the mean vorticity has a component parallel to the pure-skewing direction of 45° to the x-axis). Thus, one can obtain that for the coordinate system used in Figure 13, the mean velocity should satisfy $\overline{u}_n = -\tan(\theta + 2\alpha)(\overline{u}_s - (\overline{u}_s)_c)$, where $\tan\theta = \tan\beta\cos 2\alpha/(1 + \tan\beta\sin 2\alpha)$, and $\beta = 45 - 26 = 19°$ is the difference between the collateral flow and pure skewing directions. Measured clockwise from the horizontal axis, the predicted angles for Cases TS1 and TS2 are 43 and −8°, respectively, both of which are fairly close to the values observed in Figure 13. The behavior of q^2 (Figure 14a), and therefore, a_1 (Figure 14b) depends upon whether the effect of the mean strain represents that of an adverse or favorable pressure gradient. The kinetic energy increases, and structure parameter decreases, for the decelerating-strain flow, Case TS1; for Case TS2 the opposite occurs.

Conclusions

A DNS study of nonequilibrium 3DBLs indicates that for the shear-driven case, the greatest decrease in mean turbulent drag is obtained when a spanwise shear is applied in the region between $5 \le y^+ \le 15$; it is postulated that this result is related to the observation that maximum turbulence suppression occurs for boundary layers above oscillating surfaces when the spanwise-oscillation period is about $T^+ = 100$. The qualitatively different influence of suddenly applied spanwise and streamwise wall

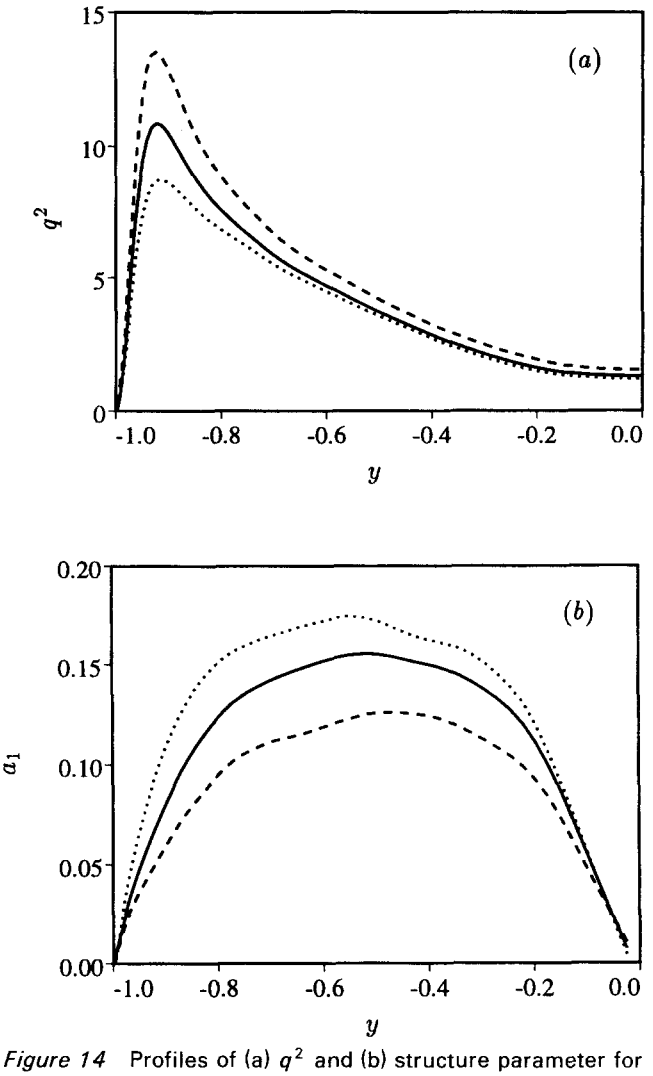

Figure 14 Profiles of (a) q^2 and (b) structure parameter for Cases TS1 and TS2; symbols as in Figure 13

shears on, for example, enstrophy profiles implies that nonequilibrium boundary layers produced by an abrupt mean-flow change are sensitive to the type—and not just the suddenness—of that change. Investigation of the pressure-driven flow using strained-channel simulations has begun to yield insight into differences between the two main versions of 3DBLs. In the future, we plan to continue this effort by considering less-rapid strain rates than that imposed here and utilize initial fields aligned at various orientations in order to isolate adverse pressure gradient and pure-skewing effects. An attempt will also be made to determine the Reynolds number dependence of our conclusions regarding the shear-driven 3DBL by performing large-eddy simulations of the moving-wall flow.

Acknowledgments

This work is sponsored by the Office of Naval Research (Program Officer, L. P. Purtell). Computer resources have been supplied by the NAS program at NASA-Ames Research Center and by the San Diego Supercomputer Center. We have benefited from discussions with P. Spalart and P. Bradshaw and T. Gotoh.

References

Bradshaw, P. 1987. Turbulent secondary flows. *Annu. Rev. Fluid Mech.*, **19**, 53–74

Bradshaw, P. and Pontikos, N. S. 1985. Measurements in the turbulent boundary layer on an "infinite" swept wing. *J. Fluid Mech.*, **159**, 105–130

Driver, D. M. and Hebbar, S. K. 1991. Three-dimensional turbulent boundary-layer flow over a spinning cylinder. NASA TM 102240

Eaton, J. K. 1995. Effects of mean flow three-dimensionality on turbulent boundary-layer structure. *AIAA J.*, **33**, 2020–2025

Furuya, Y., Nakamura, I. and Kawachi, H. 1966. The experiment on the skewed boundary layer on a rotating body. *Bull. Japan. Soc. Mech. Eng.*, **9**, 702–710

Jiménez, J. and Moin, P. 1991. The minimal flow unit in near-wall turbulence. *J. Fluid Mech.*, **225**, 213–240

Jung, W. J., Mangiavacchi, N. and Akhavan, R. 1992. Suppression of turbulence in wall-bounded flows by high-frequency spanwise oscillations. *Phys. Fluids*, **4**, 1605–1607

Kim, J., Moin, P. and Moser, R. 1987. Turbulence statistics in fully developed channel flow at low-Reynolds number. *J. Fluid Mech.*, **177**, 133–166

Laadhari, F., Skandaji, L. and Morel, R. 1994. Turbulence reduction in a boundary layer by a local spanwise oscillating surface. *Phys. Fluids*, **6**, 3218–3220

Lohmann, R. P. 1976. The response of a developed turbulent boundary layer to local transverse surface motion. *J. Fluids Eng.*, **98**, 354–363

Moin, P., Shih, T.-H., Driver, D. M. and Mansour, N. N. 1990. Direct numerical simulation of a three-dimensional turbulent boundary layer. *Phys. Fluids*, **2**, 1846–1853

Rogallo, R. S., 1981. Numerical experiments in homogeneous turbulence. NASA TM 81315

Schwarz, W. R. and Bradshaw, P. 1994. Turbulence structural changes for a three-dimensional turbulent boundary layer in a 30° bend. *J. Fluid Mech.*, **272**, 183–209

Sendstad, O. and Moin, P. 1992. The near-wall mechanics of three-dimensional turbulent boundary layers. Report No. TF-57, Thermosciences Div., Dept. Mech. Engr., Stanford Univ., Stanford, CA